UNIVERSITY OF MINNESOTA
ST. ANTHONY FALLS HYDRAULIC LABORATORY

Project Report No. 144

The Generation of Internal Waves in Stratified Fluids

by
CHARLES C. S. SONG
and
JACK C. HWANG

This research was sponsored by the Office of Naval Research, Department of the Navy, under Contract N00014-67-A-0113-0003, NR 062-388.

JUNE 1973
MINNEAPOLIS, MINNESOTA

CONTENTS

LIST OF ILLUSTRATIONS

PREFACE

The material presented herein is largely taken from the Ph.D. thesis of Jack C. Hwang, which was submitted to the Graduate School of the University of Minnesota in March of 1973. The work was conducted during the period July 1, 1969, through February 28, 1973 and was supported by the Office of Naval Research, U.S. Navy, under the terms of Contract N00014-67-A-0113-0003. Some supplemental computer time was granted to the project at no cost by the University of Minnesota Computer Center. The authors are very grateful to the Navy and the University for their support.

ABSTRACT

Internal waves in exponentially stratified fluids confined between two parallel boundaries have been studied analytically and experimentally with both a fixed and a free upper surface.

In the analytical model, waves were generated by vortex-like or source-like oscillatory disturbances. A modified image method was developed according to the principle of superposition using Hurley's elementary solutions for unbounded fluid. A basic image system which satisfies the wall boundary condition and is free of singularities in the flow field was found for every elementary vortex or source located anywhere in the field. The internal wave associated with this image system is intimately related to the characteristic mesh of the system. Only the first mode of the progressive internal wave is possible when the elementary vortex or source is located on the centerline of the channel. It appears that eccentrically located disturbances are required to generate higher mode internal waves, although numerical analysis has not been carried out for this case.

An experiment was carried out in a channel filled with salt water of exponential density stratification. A rigid flat plate wave generator and a flexible rubber diaphragm wave generator located at mid-depth, both oscillating in a vertical direction, were used. Excellent agreement was obtained between the predicted and the measured wave length. The predicted wave shape and the measured wave shape were also in good agreement. Less complete agreement was obtained for the case of wave amplitude, however.

THE GENERATION OF INTERNAL WAVES IN STRATIFIED FLUIDS

1. INTRODUCTION

In the laboratory, the standard method of generating internal waves in a stratified fluid is oscillation of a solid body. For example, Keulegan and Carpenter (1961)* generated interfacial progressive waves in a two-layer system by oscillating a horizontal plate located at the interface. In this way it was possible to generate the interfacial wave without exciting the surface waves. When there are n layers, there are n possible modes of progressive waves associated with the system (Greenhill, 1887). In general, for a continuously stratified fluid bounded by either two solid walls or a solid wall and a free surface, there exist infinitely many modes of internal progressive waves; see Lamb (1932) and Yih (1965). How these possible modes of internal waves can be selectively excited in a laboratory test facility is a problem which appears to have escaped the attention of past investigators. The capacity to selectively excite different modes of internal waves is necessary if laboratory simulation of naturally occurring internal waves is to be attempted.

Some analytical and experimental work has been carried out as a first step toward the goal of achieving the selective excitation of internal waves in stratified fluid. The analytical part of the work can be considered an extension of Hurley's work (1969) on the use of source- and vortex-like elementary solutions. Using a characteristic transformation, Hurley was able to transform the linearized partial differential equations for entropy or pressure for the case of exponential stratification to Bessel's equation of zero order. A solution of this equation in unconfined fluid behaves like a source or a vortex

---

*References are listed alphabetically on page 23.

near the origin and like a progressive wave at a large distance from it. Using the principle of superposition, he then proceeded to solve the problem of oscillating cylinders in an unconfined and exponentially stratified fluid.

It is shown in this paper that the method of images which has been used extensively for potential flows of homogeneous fluids can also be used for the case of exponentially stratified fluid. The boundary condition of parallel walls can be satisfied by using a column of infinitely many singularities. However, since the basic source or vortex solution is singular along the two characteristic lines, the single column distribution would result in unrealistic velocity distribution. The undesirable singularities along the characteristic lines were eliminated by using a system of singularities distributed along three columns. The numerical results indicate that the wave lengths, and thus the wave modes, of the emitted internal waves are determined by the spacing of the image systems. Also discussed in this paper is the experimental result, which tends to confirm the computational result.

2. BASIC SOLUTIONS IN UNBOUNDED FLUID

Although the theory described herein is applicable to the isentropic flow case, the discussion will be limited to the incompressible fluid case. The Euler equations of motion and the equation of continuity for the two-dimensional flow of a stratified fluid are

$$\frac{\partial u}{\partial t} + u\frac{\partial u}{\partial x} + v\frac{\partial u}{\partial v} = -\frac{1}{\rho}\frac{\partial p}{\partial x} \tag{2.1}$$

$$\frac{\partial v}{\partial t} + u\frac{\partial v}{\partial x} + v\frac{\partial v}{\partial y} = -\frac{1}{\rho}\frac{\partial p}{\partial y} - g \tag{2.2}$$

$$\frac{\partial \rho}{\partial t} + \frac{\partial}{\partial x}(\rho u) + \frac{\partial}{\partial y}(\rho v) = 0 \tag{2.3}$$

Here x, y is the set of rectangular coordinates with gravity acting in the direction of $-y$, u and v are the corresponding velocity components, ρ is the density, p is the pressure, and g is the gravitational acceleration. The condition of incompressibility

$$\frac{\partial \rho}{\partial t} + u \frac{\partial \rho}{\partial x} + v \frac{\partial \rho}{\partial y} = 0 \tag{2.4}$$

reduces Eq. (2.3) to

$$\frac{\partial u}{\partial x} + \frac{\partial v}{\partial y} = 0 \tag{2.5}$$

Thus a stream function ψ exists such that

$$u = -\frac{\partial \psi}{\partial y}, \quad v = \frac{\partial \psi}{\partial x} \tag{2.6}$$

Suppose that small motions are taking place in the fluid, and the pressure and density are written as

$$p = p_o + p_1, \quad \rho = \rho_o + \rho_1$$

in which the subscript o represents the equilibrium values which are assumed to be functions of y only and the subscript 1 represents the perturbation quantities.

Velocity components and perturbation quantities are regarded as small quantities. If small quantities of the second order are neglected, Eqs. (2.1) through (2.3) reduce to

$$\rho_o \frac{\partial u}{\partial t} = -\frac{\partial p_1}{\partial x} \tag{2.7}$$

$$\rho_o \frac{\partial v}{\partial t} = -\frac{\partial p_1}{\partial y} - g\rho_1 \tag{2.8}$$

$$\frac{\partial \rho_1}{\partial t} + v \frac{\partial \rho_o}{\partial y} = 0 \tag{2.9}$$

By eliminating p_1 and ϱ_1 from the above equations and using the stream function, we find that

$$\nabla^2\ddot{\psi} + \frac{1}{\varrho_o}\frac{\partial\varrho_o}{\partial y}\left(\frac{\partial\ddot{\psi}}{\partial y} - g\,\frac{\partial^2\psi}{\partial x^2}\right) = 0 \tag{2.10}$$

in which the dots denote differentiation with time. This equation was derived by Lamb (1932).

Considering an oscillatory disturbance and writing

$$\psi = \psi_o(x,y)\ \exp(-\ i\,\omega t) \tag{2.11}$$

Eq. (2.10) reduces to

$$\frac{\partial^2\psi_o}{\partial y^2} - \eta^2\,\frac{\partial^2\psi_o}{\partial x^2} + \frac{1}{\varrho_o}\,\frac{\partial\varrho_o}{\partial y}\,\frac{\partial\psi_o}{\partial y} = 0 \tag{2.12}$$

in which

$$\eta^2 = \frac{N^2}{\omega^2} - 1, \qquad N^2 = -\,\frac{g}{\varrho_o}\,\frac{\partial\varrho_o}{\partial y}$$

and N is known as the Brunt-Väisälä frequency or the characteristic frequency.

Equation (2.12) is hyperbolic when $\omega < N$ and thus the emission of internal waves is possible when the disturbance frequency is less than the characteristic frequency. For a stably and exponentially stratified fluid with a constant stratification factor of β,

$$\varrho_o = \varrho_o^{\,*}\ \exp(-\ \beta y)$$

and the characteristic frequency $N = \sqrt{g\beta}$ is constant everywhere.

Hurley (1969) used the following transformations to transform the governing equation of the perturbation pressure into Bessel's equation of zero order:

$$\zeta^2 = \frac{\beta^2}{4\eta^2}(x^2 - \eta^2 y^2) \tag{2.13}$$

and

$$\psi_o = \exp(\tfrac{1}{2}\beta y)\, f(\zeta) \tag{2.14}$$

These equations also transform the governing equation in ψ_o, Eq. (2.12), into Bessel's equation of zero order,

$$\frac{d^2 f}{d\zeta^2} + \frac{1}{\zeta}\frac{df}{d\zeta} + f = 0 \tag{2.15}$$

The general solution of Eq. (2.15) can be written as the linear combination of Hankel functions of the first kind, $H_o^{(1)}(\zeta)$, and the second kind, $H_o^{(2)}(\zeta)$. Since a Hankel function of the second kind results in unbounded velocity as $x \to \pm\infty$, this solution must be dropped on physical grounds. Thus only

$$f(\zeta) = mH_o^{(1)}(\zeta) \tag{2.16}$$

will be considered. The arbitrary constant m is a strength factor which will be taken as unity for the sake of simplicity.

Since ζ as defined by Eq. (2.13) has branch cuts along the characteristic lines

$$x \pm \eta y = 0 \tag{2.17}$$

the value of ζ in the region where $x^2 - \eta^2 y^2 < 0$ will be chosen as $\zeta = i|\zeta|$. Omitting the exponential time factor, the velocity components can be written as

$$u = -\frac{\beta}{2}\exp(\tfrac{1}{2}\beta y)[H_o^{(1)}(\zeta) + \frac{\beta y}{2\zeta} H_1^{(1)}(\zeta)] \tag{2.18}$$

$$v = -\frac{\beta^2}{4\eta^2}\exp(\tfrac{1}{2}\beta y)[\frac{x}{\zeta} H_1^{(1)}(\zeta)] \tag{2.19}$$

In the neighborhood of small $|\zeta|$, the Hankel functions are singular and have the following expansions:

$$H_o^{(1)}(\zeta) \sim \frac{2i}{\pi} J_o(\zeta) \ln \frac{\zeta}{2} + \ldots \qquad (2.20)$$

$$H_1^{(1)}(\zeta) \sim \frac{2i}{\pi} [- \frac{1}{\zeta} + J_1(\zeta) \ln \frac{\zeta}{2} + \ldots] \qquad (2.21)$$

Thus the velocity components have a first order and a logarithmic singularity along the characteristic lines. The streamline pattern in the neighborhood of the characteristic lines is sketched in Fig. 1. It is seen that the characteristic lines are like the traces of vortex sheets except that the velocity jumps by an infinite amount across these lines.

For large ζ, the Hankel functions have the following asymptotic values:

$$H_o^{(1)}(\zeta) \sim \sqrt{\frac{2}{\pi\zeta}} \exp[i(\zeta - \frac{\pi}{4})] \qquad (2.22)$$

$$H_1^{(1)}(\zeta) \sim \sqrt{\frac{2}{\pi\zeta}} \exp[i(\zeta - \frac{3\pi}{4})] \qquad (2.23)$$

For example, the velocity components of a point located on $y = 0$ at large x are

$$v \sim - \sqrt{\frac{\beta}{\pi\eta x}} \exp[i(\frac{\beta}{2\eta} x - \omega t - \frac{3\pi}{4})] \qquad (2.24)$$

$$u \sim - \sqrt{\frac{\beta\eta}{\pi x}} \exp[i(\frac{\beta}{2\eta} x - \omega t - \frac{\pi}{4})] \qquad (2.25)$$

indicating that the flow is that of a progressive wave of decreasing amplitude. The wave length λ is

$$\lambda = \frac{4\pi\eta}{\beta} \qquad (2.26)$$

Instead of working with the stream function, it is possible to use the perturbation pressure p_1 as the dependent variable. For an oscillatory disturbance in an exponentially stratified fluid the governing equation becomes

$$\frac{\partial^2 p_1^*}{\partial y^2} - \eta^2 \frac{\partial^2 p_1^*}{\partial x^2} + \beta \frac{\partial p_1^*}{\partial y} = 0 \tag{2.27}$$

where p_1^* is defined

$$p_1 = p_1^* \exp(-i\omega t) \tag{2.28}$$

Neglecting the exponential time factor, the velocity components are related to the pressure as follows:

$$u = -\frac{i}{\varrho_o \omega} \frac{\partial p_1^*}{\partial x} \tag{2.29}$$

$$v = \frac{i}{\varrho_o \omega \eta^2} \frac{\partial p_1^*}{\partial y} \tag{2.30}$$

Equation (2.27) is identical in form to Eq. (2.12). Therefore the procedure used before can be adapted to find the solution for p_1^*. Since the solution is identical to that obtained by Hurley (1969) and is discussed extensively by him, it will not be presented in detail here. Suffice it to say that the resulting flow is like that of a source in the near field and a progressive wave of decreasing amplitude with distance in the far field.

Hurley (1969) proceeded one step further and showed how the basic source- and vortex-like solutions can be used to represent the flow due to vibrating slender cylinders in an unbounded fluid. As might be expected, the solution is singular along the characteristic lines and is not valid there. For this reason, it is not known how well Hurley's solution represents the real flow.

3. INFLUENCE OF PARALLEL WALLS ON THE BASIC SOLUTIONS

When the stratified fluid is confined between two parallel walls, the solution must satisfy the additional boundary condition that the normal velocity component vanishes on the walls. For the following analysis, the x-axis is chosen so that the walls are located at $y = \pm h$. Consider a case in which a vortex of unit strength is located on the y-axis at

$$y = y_o = rh, \quad -1 < r < 1 \tag{3.1}$$

It can readily be shown that the image system that satisfies the boundary condition on the walls is given by

$$\psi = \Psi(0,y_o) = \exp[\tfrac{1}{2}\beta(y - y_o)][H_o^{(1)}(\zeta_o) + \sum_{n=1}^{\infty} (-1)^n H_o^{(1)}(\zeta_n) + \sum_{n=1}^{\infty} (-1)^n H_o^{(1)}(\zeta_n')] \tag{3.2}$$

in which

$$\zeta_n^2 = \frac{\beta^2}{4\eta^2}[x^2 - \eta^2(y - y_n)^2] \tag{3.3}$$

$$(\zeta_n')^2 = \frac{\beta^2}{4\eta^2}[x^2 - \eta^2(y - y_n')^2] \tag{3.4}$$

$$y_n = [2n + (-1)^n r]h \tag{3.5}$$

$$y_n' = -[2n - (-1)^n r]h \tag{3.6}$$

Equation (3.2) represents the stream function due to a column of vortices located on the y-axis as shown in Fig. 2. In general, for a unit vortex located at (x_o,y_o), the required image system is

$$\psi = \Psi(x_o,y_o) \tag{3.7}$$

which is obtained from Eq. (3.2) by replacing x with $x - x_o$.

Since there are two characteristic lines associated with each vortex, there are infinitely many characteristic lines, as shown in Fig. 2. On each of these lines the velocity is singular. Since the velocity must remain finite in the actual flow field, the single column of the vortex system located on the y-axis and given by Eq. (3.2) is unsatisfactory on physical grounds. A way must be found to eliminate the singularities along the characteristic lines. The pattern of characteristic lines shown in Fig. 2 suggests the possibility of using additional columns of vortex systems located at the nodal points of the characteristic mesh. One possibility is to use two additional columns of nodal points next to the y-axis as shown in Fig. 2. Let the strengths of these image systems be a and b, and write

$$\psi = \Psi(0,y_o) + a\Psi(x_o,-y_o) + b\Psi(-x_o,-y_o) \tag{3.8}$$

where

$$x_o = 2\eta h \tag{3.9}$$

It is necessary to determine the strength factors a and b which will result in canceling both the first order and the logarithmic singularities in the velocity components. It can readily be shown that the required strength factors are

$$a = b = \frac{1}{2} \exp(-\beta rh) \tag{3.10}$$

The required solution, free of singularities in the region $|x - x_o| > 0$, is thus

$$\psi = \Psi(0,y_o) + \frac{1}{2} \exp(-\beta rh)[\Psi(x_o,-y_o) + \Psi(-x_o,-y_o)] \tag{3.11}$$

The corresponding velocity components are obtained by differentiating Eq. (3.11) according to the definition of the stream function.

The image system for a source located at $(0,rh)$ between two parallel walls, as depicted in Fig. 2, can be obtained in a slightly different manner. A source of unit strength located at $(0,y_o)$ is given by

$$p_1^* = \exp[-\tfrac{1}{2}\beta(y - y_o)]H_o^{(1)}(\zeta_o) \tag{3.12}$$

where ζ_o is given by Eq. (3.3). The corresponding velocity components are obtained by differentiation according to Eqs. (2.29) and (2.30). The vertical velocity component which is obtained by differentiation of Eq. (3.12) with respect to y contains Hankel's functions of the first and second orders. For this reason, the boundary condition on the walls cannot be satisfied by using the image system arranged in the manner shown in Fig. 2. To cancel the additional term involved in v, an additional image system is required. The key to finding such an image system is found in the form of Eq. (2.30). This equation suggests that the vertical velocity component resulting from a distributed source along a line parallel to the y-axis is equivalent to p_1^* of a concentrated source; that is, by integrating Eq. (2.30),

$$\int_{y_o}^{y_1} v(x,y-\tau)d\tau = \frac{i}{\omega\eta^2}\int_{y_o}^{y_1} \frac{1}{\varrho_o(y-\tau)} \frac{\partial p_1^*(y-\tau)}{\partial y} d\tau$$

For example, consider a unit source at $(0,y_o)$ and its image at $(0,y_1)$ having a strength a. To this system we now add a distributed source of strength b per unit length along the line joining the two points. The equations for the vertical velocity component due to the original source, the image source, and the distributed source are, respectively,

$$v(0,y_o) = \frac{i}{\varrho_o^*\omega\eta^2}\exp[\tfrac{1}{2}\beta(y - y_o)][-\tfrac{\beta}{2}H_o^{(1)}(\zeta_o) + \frac{\beta^2(y - y_o)}{2\zeta_o}H_1^{(1)}(\zeta_o)] \tag{3.13}$$

$$v(0,y_1) = \frac{ia}{\varrho_o^*\omega\eta^2}\exp[\tfrac{1}{2}\beta(y - y_1)][-\tfrac{\beta}{2}H_o^{(1)}(\zeta_1) + \frac{\beta^2(y - y_1)}{2\zeta_1}H_1^{(1)}(\zeta_1)] \tag{3.14}$$

$$v(0,y_o<y<y_1) = \frac{ib}{\varrho_o^*\omega\eta^2}\left\{\exp[\tfrac{1}{2}(y - y_1)]H_o^{(1)}(\zeta_1) - \exp[\tfrac{1}{2}(y - y_o)]H_o^{(1)}(\zeta_o)\right\} \tag{3.15}$$

When $y_0 = rh$ and $y_1 = (2 - r)h$, it is possible to determine a and b such that the resulting vertical velocity component vanishes on $y = h$. Proceeding in this manner, it is possible to show that the boundary conditions on the parallel walls can be satisfied by a column of discrete sources and a distributed source on a vertical line. Again the singularities on each of the infinitely many characteristic lines can be canceled by using a 3-column system in exactly the same manner as in the case of the vortex solution. More detailed discussion concerning distributed sources can be found in Hwang (1973).

4. NUMERICAL EXAMPLES - VORTEX IN THE MIDDLE OF A CHANNEL

In order to visualize and further understanding of the flows represented by the image systems discussed in the previous section, numerical computations were carried out for the vortex system due to a primary vortex located at the middle of a channel, $r = 0$.

In this particular case the vertical and horizontal distances between the characteristic nodal points are $2h$ and $2\eta h$, respectively, and all characteristic meshes are congruent. Therefore, it is convenient to use dimensionless scales defined as

$$\bar{x} = \frac{x}{2\eta h}, \quad \bar{y} = \frac{y}{2h} \tag{4.1}$$

so that

$$\zeta^2 = \beta h(\bar{x}^2 - \bar{y}^2) \tag{4.2}$$

The velocity components are made dimensionless in the following way:

$$v = -\frac{\beta}{\eta}\bar{v}, \quad u = -\frac{\beta}{2}\bar{u} \tag{4.3}$$

It should be noted here that the strength factor of ψ as defined by Eq. (3.11) has a dimension of L^2/T and Eq. (4.3) is dimensionally correct. Equation (4.2) clearly indicates that the flow pattern depends only on βh, which we shall call the "dimensionless stratification factor." The infinite series representing the image system converges very slowly when βh is very small. For this reason, only two cases, in which $\beta h = 0.5$ and 0.75, were computed.

4.1 Flow in the Far Field, $\bar{x} > 1$

Since the flow is symmetrical with respect to the y-axis, only the region where $\bar{x} > 0$ will be considered. Furthermore, for the purpose of numerical computation and interpretation of the results it is convenient to separate the flow field into the near field, $\bar{x} < 1$, and the far field, $\bar{x} > 1$. The function represented by Eq. (3.11) is regular everywhere in the far field, and the computation is quite straightforward. For example, the real and imaginary parts of the dimensionless vertical velocity component, $\bar{v}_R$ and $\bar{v}_I$, for the $\beta h = 0.50$ case are plotted in Fig. 3. The profiles are nearly, but not exactly, symmetrical with respect to the $\bar{x}$-axis. The corresponding velocity profiles on the centerline of the channel, $\bar{y} = 0$, are shown in Fig. 4. The velocity profiles shown in Fig. 4 are nearly sinusoidal.

Having obtained the distribution of the vertical velocity component, it is now possible to calculate the wave profile in the far field. For the case of the flow due to an oscillatory disturbance considered herein, Eq. (2.9) reduces to

$$\rho_1 = \frac{i\beta\, \rho_o\, v}{\omega} \tag{4.4}$$

Therefore, the density distribution at any instant is, by definition,

$$\rho = \rho_o\left(1 + \frac{i\beta v}{\omega}\right) \tag{4.5}$$

As usual, only the real part of the above equation is related to the physical quantity. Since the density of a given fluid particle remains constant at all times, the trajectory of a particle is obtained by setting the right-hand side of Eq. (4.5) equal to a constant appropriate for that particle. For example, the trajectories of all the particles with their neutral positions on $\bar{y} = 0$ are determined by setting ϱ equal to ϱ_o^*. Thus the wave profile consisting of all the particles whose neutral positions are on the $\bar{x}$-axis is

$$1 + \frac{\beta^2}{\eta\omega}(\bar{v}_I \cos\omega t - \bar{v}_R \sin\omega t) = \exp(\beta h\, \bar{y}) \tag{4.6}$$

The wave profile computed for the case of $\beta h = 0.50$ at an instant $t = 0$ is shown in Fig. 5.

It is noteworthy that both the wave profile shown in Fig. 5 and the velocity profiles shown in Fig. 4 are nearly sinusoidal and have a wave length of $4\eta h$. Indeed, least-square fitting of these curves with sinusoidal curves of wave length $4\eta h$ gives standard deviations of less than one per cent. For a very weak stratification, the right-hand side of Eq. (4.6) can be expanded into a power series of $\beta h\bar{y}$. Assuming small amplitude waves and approximating $\bar{v}_I$ and $\bar{v}_R$ using the corresponding values on $\bar{y} = 0$, Eq. (4.6) is approximated by

$$\bar{y} = \frac{m\beta}{\eta h\omega}|\bar{v}|\cos(\pi\bar{x} - \omega t) \tag{4.7}$$

in which m is the strength of the vortex having the dimension of L^2/T and $|\bar{v}|$ is the amplitude of the vertical velocity component on $\bar{y} = 0$ due to a unit strength vortex system. Clearly, the flow in the far field is that of a progressive wave of constant amplitude and wave length

$$\lambda = 4\eta h \tag{4.8}$$

4.2 Flow in the Near Field, $\bar{x} < 1$

Unlike the flow in the far field, the flow in the near field is not completely free of singularities. Of considerable significance is the fact that the velocity has a finite jump across the characteristic lines marked $\overline{ab}$ and $\overline{ac}$ in Fig. 6. For this reason, it is possible to regard these lines as a wedge-shaped oscillatory boundary. With this interpretation given to the near field flow, it suffices to investigate only the normal components of the velocity on the wedge-shaped boundary having a vertex angle θ given by

$$\theta = 2 \tan^{-1} \frac{1}{2\eta} \tag{4.9}$$

With $\vec{n}_1$ and $\vec{n}_2$ denoting the outward normal vectors on $\overline{ab}$ and $\overline{ac}$, respectively, we have

$$\vec{n}_1 = \frac{\vec{i} + \eta\vec{j}}{\sqrt{1 + \eta^2}} \quad \text{and} \quad \vec{n}_2 = \frac{\vec{i} - \eta\vec{j}}{\sqrt{1 + \eta^2}} \tag{4.10}$$

Here $\vec{i}$ and $\vec{j}$ are unit vectors in the direction of the x-axis and the y-axis, respectively. The velocity of a fluid particle is

$$\vec{v} = u\vec{i} + v\vec{j} \tag{4.11}$$

and, hence, the normal component of the velocity is

$$v_{n1} = \vec{n}_1 \cdot \vec{v} = - \frac{\beta}{2\sqrt{1+\eta^2}} [2\bar{v}_R + \bar{u}_R + i(2\bar{v}_I + \bar{u}_I)] \tag{4.12}$$

on $\overline{ab}$ and

$$v_{n2} = \frac{\beta}{2\sqrt{1+\eta^2}} [2\bar{v}_R - \bar{u}_R + i(2\bar{v}_I - \bar{u}_I)] \tag{4.13}$$

on $\overline{ac}$.

The computed normal velocity distributions on the external surface of the wedge-shaped boundaries are shown in Figs. 7 and 8. It is seen from these figures that the motion consists of a rotational mode and a bending mode. Also, the motions of the two surfaces are almost identical and in phase.

5. EXPERIMENTAL RESULTS

5.1 General Description

Internal waves were generated by a wave generator which was located at one end of a channel 55 ft long, 6 inches wide, and 15 inches deep. At the other end of the channel an absorber made up of layers of wire screen was installed to absorb most of the wave energy and prevent wave reflection. The bottom of the channel was rigid and flat. The top of the fluid was either covered with a metal sheet to simulate a solid boundary or, for some experimental runs, left as a free surface. A schematic diagram of the experimental components is shown in Fig. 9.

Stratified fluid of a desired density profile was made possible by pumping salt water into the channel in several layers, each having a predetermined density. Successive layers decreased in density from bottom to top. Several hours after filling, molecular diffusion rounded off the sharp density gradient which initially existed between the layers. Prior to the test, samples were drawn from selected elevations and their densities measured. For a small stratification factor, the exponential stratification is practically the same as the linear stratification. A typical measured density profile and the ideal exponential stratification with $\beta = 0.03$ per ft are shown in Fig. 10. In this particular case $h = 6$ inches and the dimensionless stratification factor βh is only 0.015. Several combinations of β and h were tested.

5.2 Wave Generator

Two kinds of wave generators were used in the experiment, a rigid flat plate and a flexible rubber diaphragm, both placed horizontally and oscillated in the vertical direction. The first wave generator performs an oscillatory displacement and the second produces an oscillatory bending motion. Initially a pier was attached to the leading edge of the wave generator as shown in Fig. 9. According to Keulegan and Carpenter (1961), this was thought necessary to guide the internal wave out of the wave generator compartment. However, further tests have shown that the internal waves can be generated as well without the pier or by replacing the pier with a fixed flat plate.

The rigid flat-plate wave generator was made of sheet metal and was 18 inches long and 6 inches wide with its center connected to a plunger which was driven by a motor. Since the width of the wave generator was equal to that of the wave channel, the resulting flow should have been nearly two-dimensional. The flexible wave generator consisted of a one-foot-square rubber diaphragm attached to a solid disk 6 inches in diameter at the center. The solid disk was connected to a plunger which oscillated in the vertical direction while the edges of the rubber diaphragm were fixed to the walls of a one-foot-square wave generator compartment. A curved transition was provided between the wave generator compartment and the wave channel. A schematic diagram of the rubber diaphragm wave generator is contained in Fig. 9.

The theoretical wave generator discussed in the previous section is a wedge with a vertex angle given by Eq. (4.9), while the wave generators used in the experiment were plates. For this reason, the experimental condition does not exactly represent the theoretical condition. However, when η_1 and hence the wave length λ, is large, the theoretical wedge angle becomes small and approaches the plate condition in the limit $\eta \rightarrow \infty$. For this reason a meaningful comparison is possible, at least for the case of long waves.

5.3 Wave Measurement

An electric probe similar to that used by Lofquist (1970) was used. The probe was based on the principle that the electrical conductivity of the salt solution increases with its salinity. It consists of two thin metal plates spaced a small distance apart. The whole apparatus was insulated except for small areas on the inside surfaces near the ends of the plates. One of the plates was grounded to the bottom of the channel and the other was connected to a power source. As the waves passed through the probe, the conductivity between the plates changed and electrical signals were generated. As was found by Lofquist (1970), the nonlinear response of the probe and the boundary layer effect made it very difficult to measure the wave amplitude accurately using this type of probe. For this reason, this probe was used primarily to measure the wave length and the wave speed.

Wave profile and amplitude were measured photographically. A colored oil drop, Meriam Red, which is used as a manometer fluid can be prepared for any desirable specific gravity between 1.1 and 4.0. Prior to each run, oil droplets were placed in suspension at the desired elevation. The wave profile and amplitude were measured from photographic records of the motions of the droplets.

It is inevitable that molecular diffusion continuously takes place in the prepared stratified salt solution. The wave motion may enhance the mixing. Keulegan and Carpenter (1961) reported on the distortion of internal waves after they have been running continuously for five minutes or longer. The experimental data reported herein were taken before the distortion of the waves became visible.

5.4 Experimental Data

Experimental runs were carried out for several combinations of β and h for β varying from 0.018 ft^{-1} to 0.11 ft^{-1} and h equal to 0.167 ft, 0.333 ft, and 0.50 ft. Waves were generated using both types of wave generators oscillating at different frequencies. Data were taken for the case in which the upper surface is free as well as for the case in which it is fixed. The wave generators were located at mid-depth, so that $y = 0$ at all times.

Almost perfect sinusoidal progressive internal waves were generated as long as the frequency of the wave generator oscillation was appreciably less than the characteristic frequency and the amplitude was reasonably small. Figure 11 shows a plot of the dimensionless wave length $\lambda/4h$ against the parameter η. The straight line shown in the figure is the theoretical line representing $\lambda = 4\eta h$, and the points represent all the measured values. The agreement between the theory and the data is surprisingly good considering the fact that the theoretical wave generator was a wedge while the experimental generators were plates.

The comparison of measured amplitudes with the theoretical amplitude is rather difficult for various reasons. First of all, the generator shapes and the mode of vibrations implied by the analytical result are different from those of the experiments. Secondly, the dimensionless stratification factor βh for the experiments is very small, but due to the convergence problem only fairly large βh cases were computed. Finally, a linear theory is usually not accurate in predicting the amplitude, anyway. Nevertheless, a comparison of measured and computed amplitude ratio a_W/a_G is given in

Fig. 12. Here a_W is the wave amplitude and a_G is the wave generator amplitude defined as the maximum displacement of the wave generator motions. The agreement here is not as good as in the case of wave length.

6. DISCUSSION

Rayleigh's eigen value solutions for progressive waves in an exponentially stratified fluid bounded between two parallel walls can be found in Lamb's book (1932). The condition for the existence of progressive internal waves is

$$\lambda = \frac{4\pi\eta h}{\sqrt{(\beta h)^2 + (n\pi)^2}} \tag{6.1}$$

in which n is any positive integer. For a very small stratification factor, we may neglect βh and obtain

$$\lambda = \frac{4\eta h}{n} \tag{6.2}$$

Clearly, the internal waves generated by point vortices located along the centerline of the channel as discussed in sections 4 and 5 are dominated by the first mode, $n = 1$, of all possible eigen solutions. The wave length calculated in section 4 is strongly related to the spacings of the image system or the sizes of the characteristic mesh. These spacings can be changed continuously from $2\eta h$ to zero by changing r from zero to 1, whereas the wave length given by Eq. (6.2) can take only a discrete number of values. It would be interesting to investigate this point in a future study.

If the half-depth h in Eq. (6.1) is allowed to increase indefinitely, all modes collapse to a single mode and the wave length approaches $4\pi\eta/\beta$ as a limit. This value agrees with the theoretical value of Eq. (2.26) for an isolated vortex in an infinite fluid. There is one major difference between the two solutions, however. The amplitude of an internal wave generated by a single vortex in an infinite fluid decrease as the $-1/2$ power of x due to the spreading of energy in the vertical direction, whereas the eigen solution deals with a constant-amplitude internal wave. In an exponentially stratified fluid, the characteristic lines are straight lines and the wave energy is spread between these two characteristic lines. When the fluid is confined within two walls, the energy must be reflected at the walls back into the central region while the wave amplitude is maintained constant. The image system simulates the reflective action of the boundaries by feeding wave energy into the central region from the images along the direction of the characteristic lines. Since the energy travels along the direction of the characteristic lines, and since the energy is kept in the central region through the reflective action of the walls, it is easy to visualize why the wave length is primarily determined by the sizes of the characteristic mesh. It can be reasoned, therefore, that the length of an internal wave due to an oscillatory disturbance is primarily determined by ηh and the vertical location of the disturbance represented by r.

Lamb (1932) also derived an equation for the wave length when the upper surface is a free surface. He also pointed out that the equation becomes identical to Eq. (6.1) when βh is negligibly small. This is why all the experimental data shown in Fig. 11 fall on the same line: there is no measurable influence of the upper surface condition on the wave length.

Internal waves can also be generated behind a body moving in a stratified fluid or behind a stationary body in a flowing stratified fluid. For example, the phenomenon of lee waves was studied by Long (1955), Yih (1960), and others. Long (1955) has experimentally demonstrated the existence of large-amplitude lee waves for a certain range of Froude numbers defined as

$$F_i = \frac{U}{\sqrt{g \frac{\Delta\varrho}{\varrho} H}} \tag{6.3}$$

Here U is the average speed of the approaching flow, H is the channel depth, and $\Delta\varrho$ is the fluid density difference between the bottom and the top of the channel. For an exponential stratification

$$\frac{\Delta\varrho}{\varrho} H = \beta H^2 \qquad (6.4)$$

Long (1955) also analytically determined and experimentally confirmed that the length of lee waves is given by

$$\lambda = \frac{2\pi F_i}{\sqrt{1 - (\pi F_i)^2}} \qquad (6.5)$$

Since the wave was stationary with respect to a stationary observer, it would have been moving with speed U with respect to the ambient fluid. For this reason, the lee wave becomes a progressive wave of phase velocity

$$U = \frac{\lambda\omega}{2\pi} \qquad (6.6)$$

to an observer moving with the ambient fluid. If Eqs. (6.3), (6.4), and (6.6) are substituted into Eq. (6.5) and the resulting equation is solved for λ, Eq. (4.8) is obtained; in other words, Eq. (4.8) is also an equation of wave lengths for the lee waves generated in an exponentially stratified fluid in a channel.

The task of analyzing the internal waves generated by disturbances located off-center remains to be completed. Only after this is completed can the problem of selective excitation of different modes of internal waves be solved.

7. CONCLUSIONS

An experimental and analytical study of the generation of internal waves in exponentially stratified fluid has been carried out and the results compared. The analysis is based on the superposition of source- and vortex-like elementary solutions of linearized differential equations for exponentially stratified fluid. A modified image method similar to that used for potential flow of homogeneous fluid was developed for the case of two-dimensional flows bounded by two parallel walls. An image system consisting of three columns of concentrated vortices or concentrated and distributed sources was found to closely simulate the flow of progressive internal waves generated by a wave maker. It appears that the mode of internal waves generated in a channel depends primarily on the vertical position of the disturbance. When the disturbances are located at the mid-point between the walls, the first-mode internal wave is generated. It appears that the length of the internal waves depends mainly on the sizes of the characteristic mesh of the image system.

Experimentally, internal waves were generated in a channel using a rigid flat plate or a flexible plate placed horizontally and performing oscillatory motions in the vertical direction. Nearly exponentially stratified fluids of different dimensionless stratification factors βh were tested for a number of characteristic wave lengths η. Although the theoretical wave generator is not identical with the experimental one used, very good agreement was obtained for the wave length and fair agreement was obtained for the wave amplitude. Further study is needed before selective excitations of modes other than the first mode of the internal wave can be achieved.

REFERENCES

Greenhill 1887 "Wave Motion in Hydrodynamics," American Journal of Math., Vol. IX.

Hurley, D. G. 1969 "The Emission of Internal Waves by Vibrating Cylinders," J. Fluid Mech., Vol. 36, Part 4.

Hwang, J. C. 1973 "Generation of Internal Waves in Stratified Fluid," Ph.D. Thesis, University of Minnesota.

Keulegan, Garbis H. and Carpenter, Lloyd H. 1961 An Experimental Study of Internal Progressive Oscillatory Waves, National Bureau of Standards, U.S. Department of Commerce.

Lamb, Horace 1932 Hydrodynamics, Dover Publications, pp. 378-380.

Lofquist, K. 1970 Internal Waves Produced by Spheres Moving in Density Stratified Fluid, Report 10267, National Bureau of Standards, U.S. Department of Commerce.

Long, R. R. 1955 "Some Aspects of the Flow of Stratified Fluids. III. Continuous Density Gradients," Tellus, 7, pp. 342-357.

Yih, C. S. 1960 "Exact Solutions for Steady Two-Dimensional Flow of a Stratified Fluid," J. Fluid Mech., 9, pp. 161-174.

Yih, C. S. 1965 Dynamics of Nonhomogeneous Fluids, MacMillan Book Co., pp. 29-31.

ILLUSTRATIONS

(Figures 1 through 12)

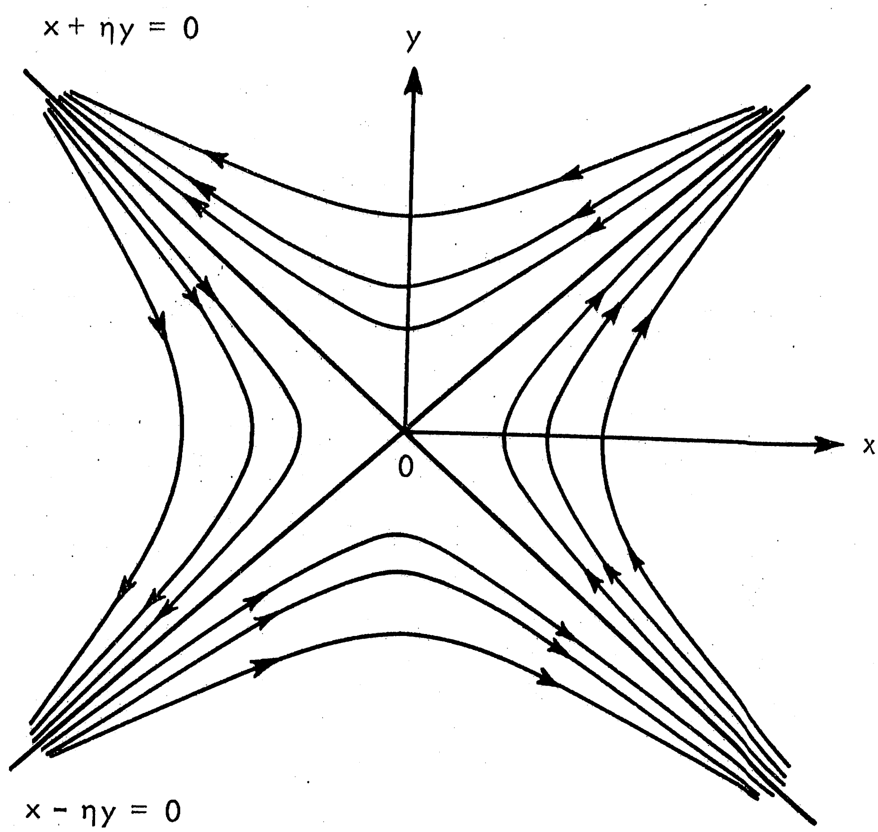

Fig. 1 - Streamline Pattern near the Origin for the Vortex-Like Solution

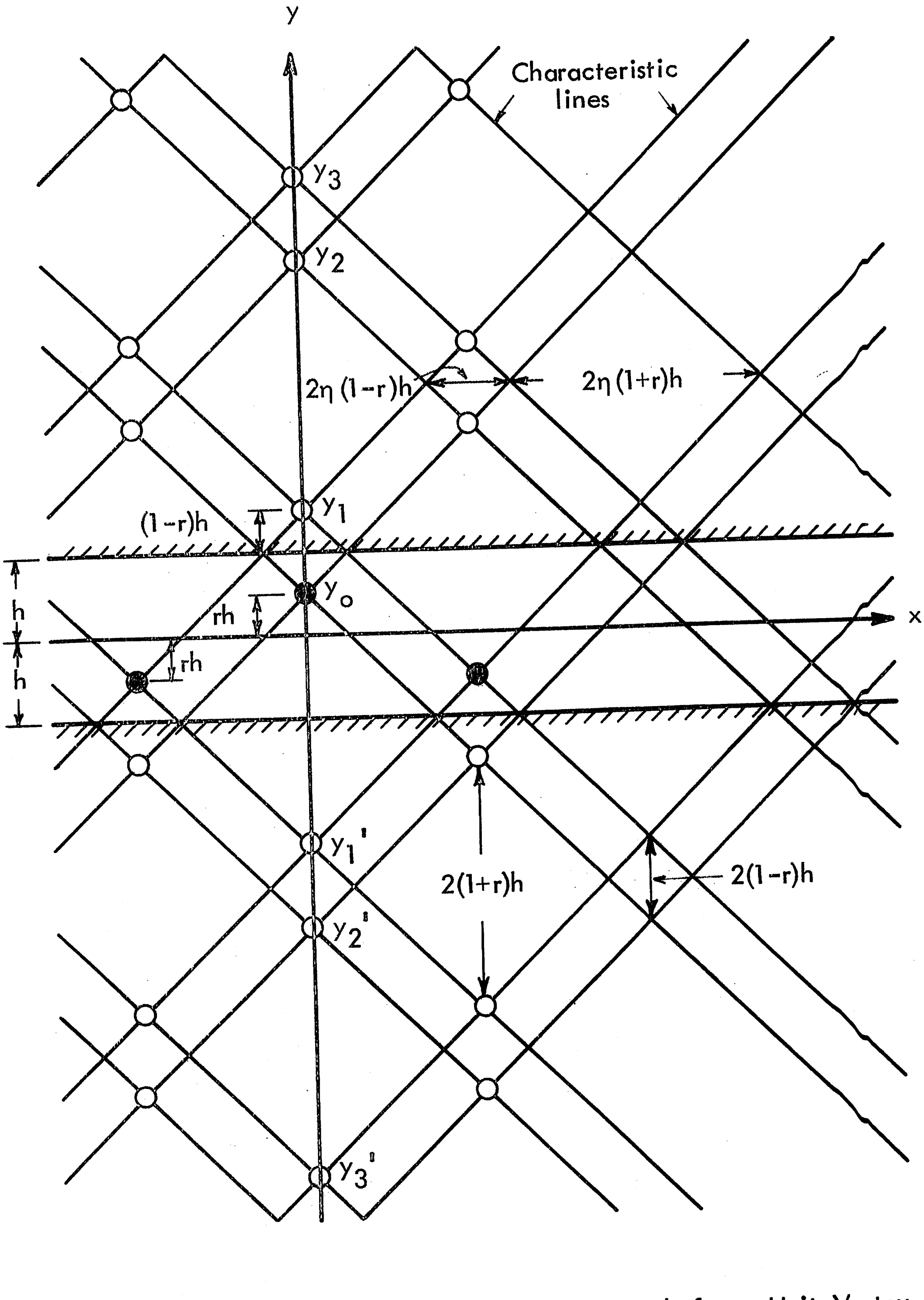

Fig. 2 - Image System and Characteristic Mesh for a Unit Vortex located at (0, rh) between two parallel walls

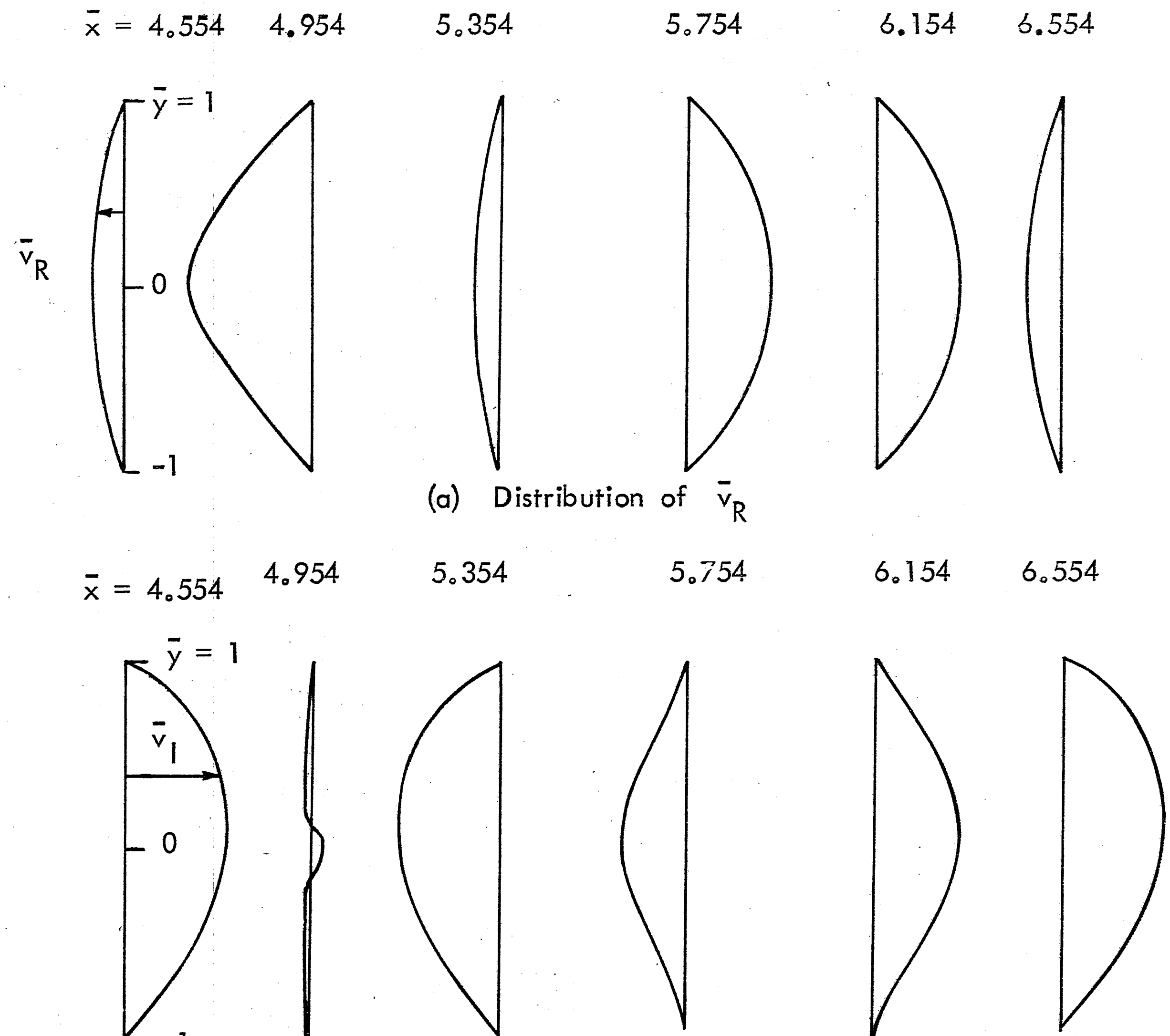

(a) Distribution of $\bar{v}_R$

(b) Distribution of $\bar{v}_I$

Fig. 3 - Vertical Velocity Component in the Far Field, $\beta h = 0.50$

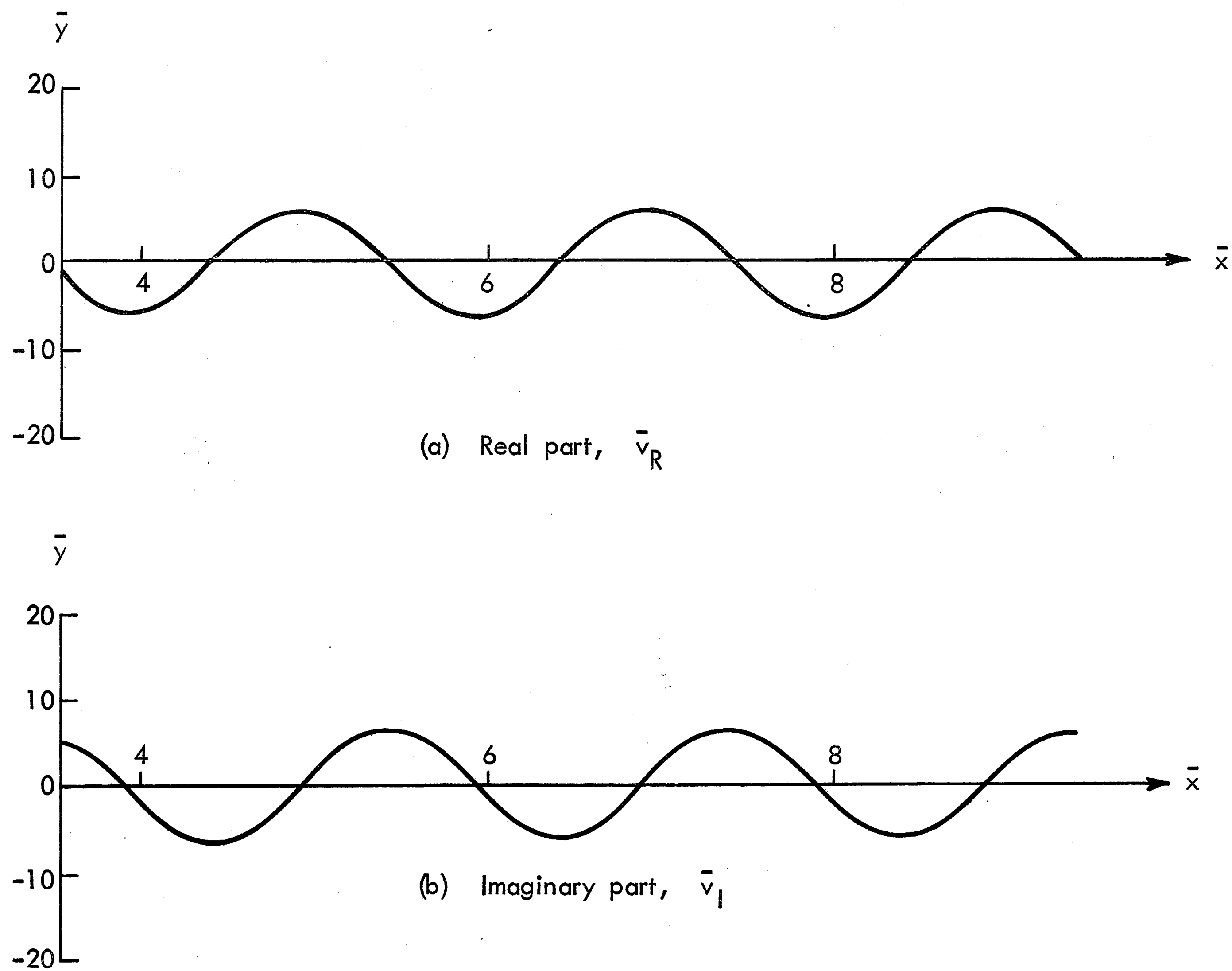

Fig. 4 - Vertical Velocity Component in the Far Field on $\bar{y} = 0$, $\beta h = 0.50$

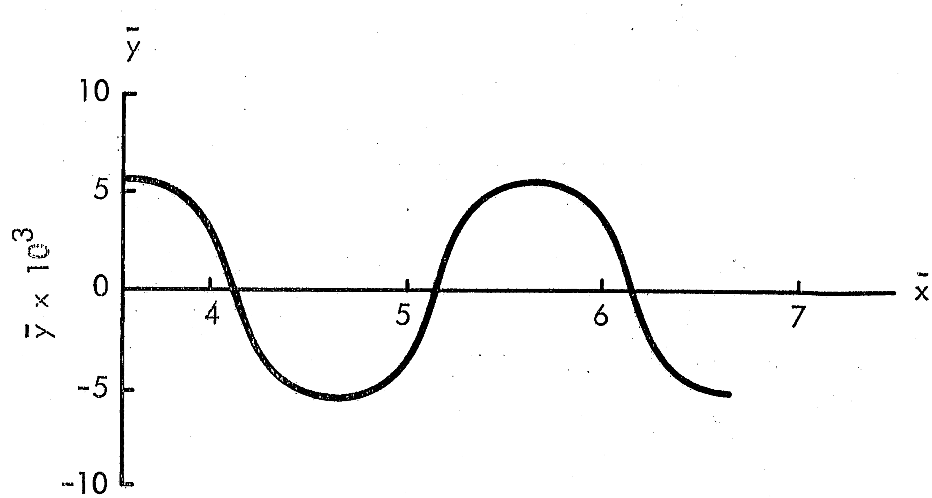

Fig. 5 - Computed Wave Profile of particles whose Neutral Positions are on $y = 0$, $\beta h = 0.50$

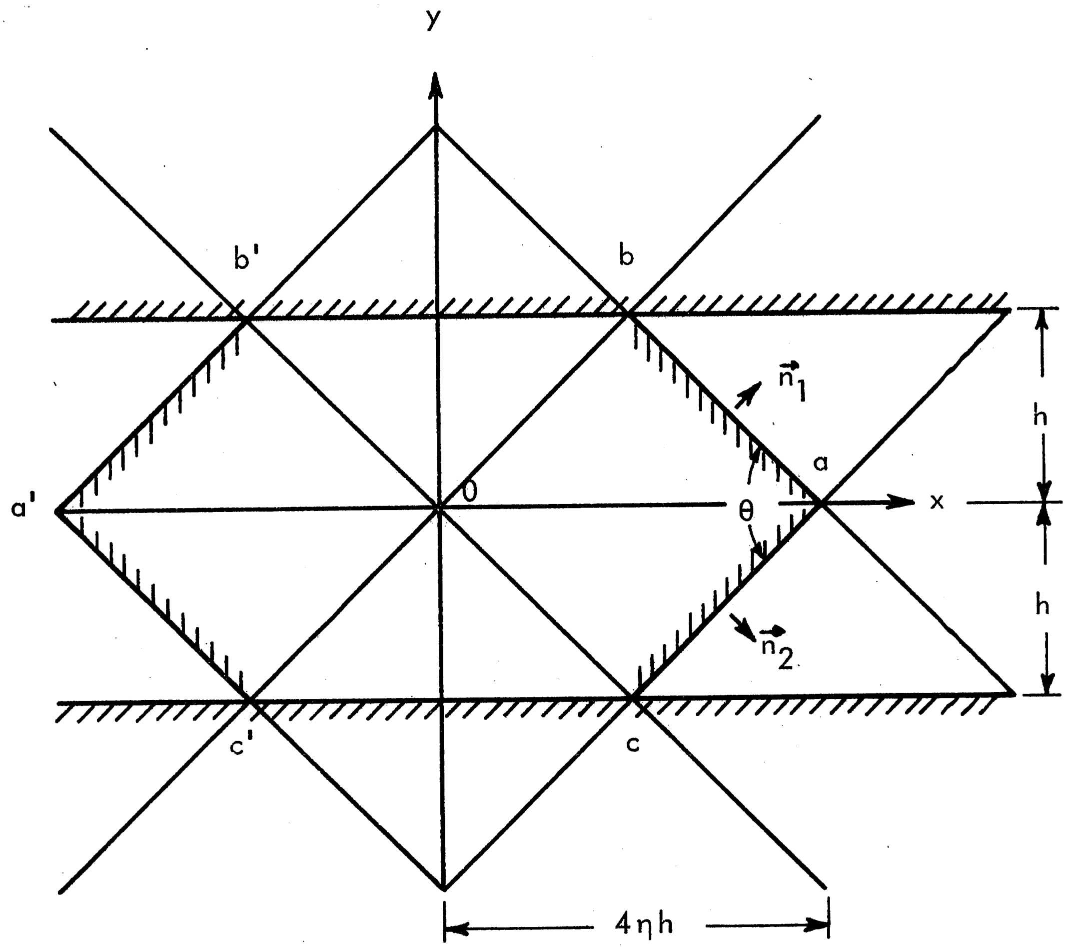

Fig. 6 - Interpretation of Flow in the Near Field, Wedge-Shaped Wave Generator

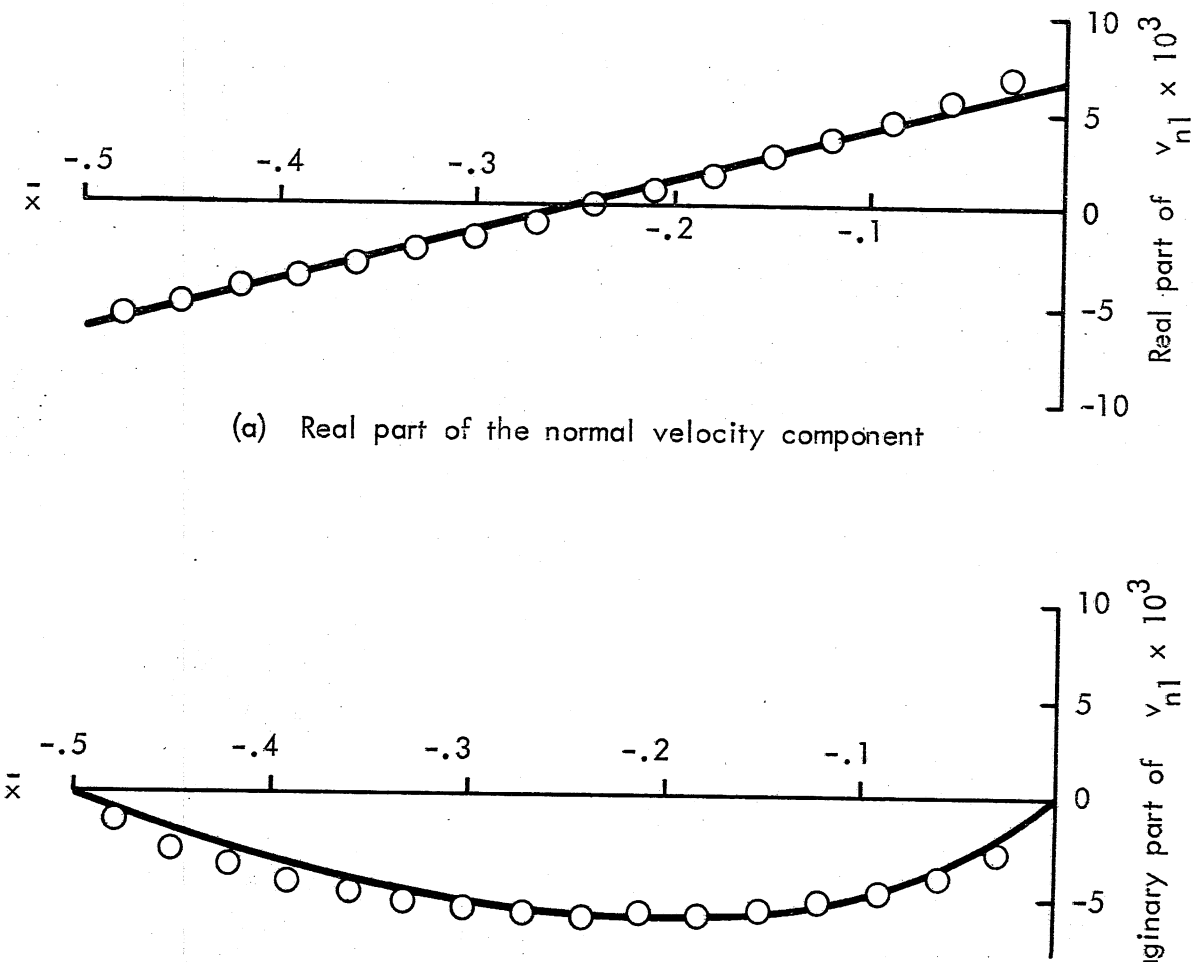

(a) Real part of the normal velocity component

(b) Imaginary part of the normal velocity component

Fig. 7 - Normal Velocity Distribution on the Upper Wedge Surface, $\beta h = 0.50$

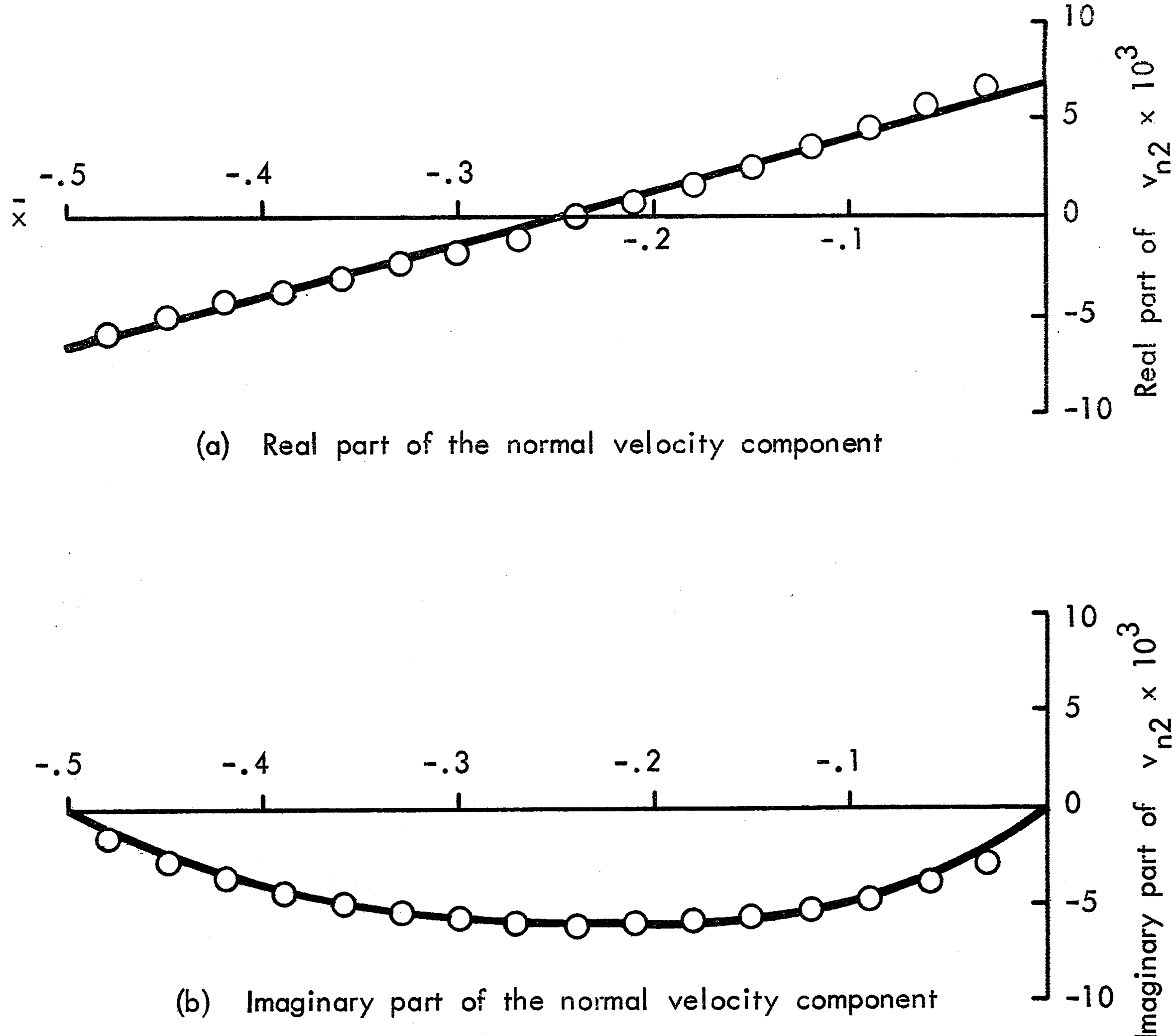

(a) Real part of the normal velocity component

(b) Imaginary part of the normal velocity component

Fig. 8 - Normal Velocity Distribution on the Lower Wedge Surface, $\beta h = 0.50$

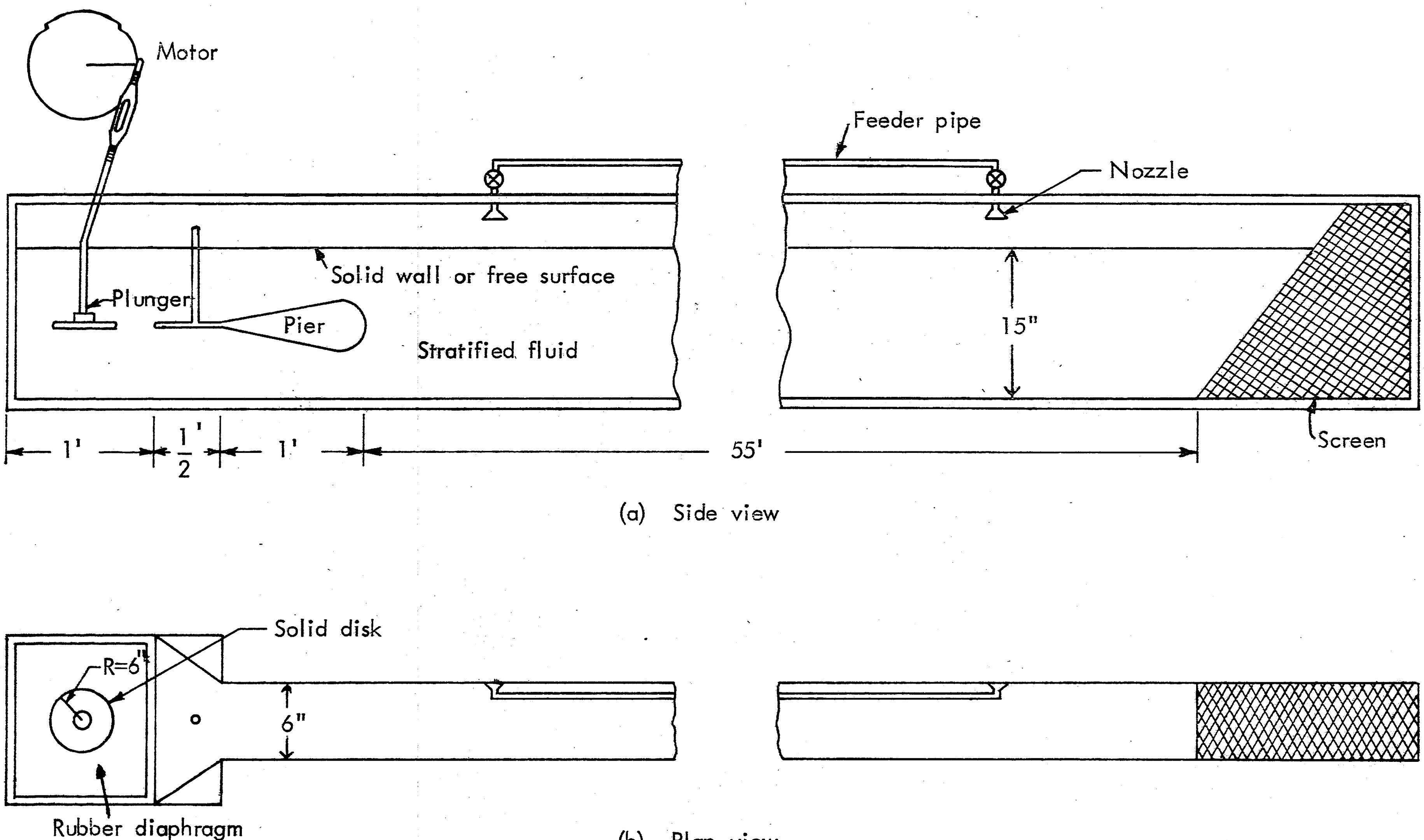

Fig. 9 - Schematic Diagram of the Side and Plan View of the Experimental Components

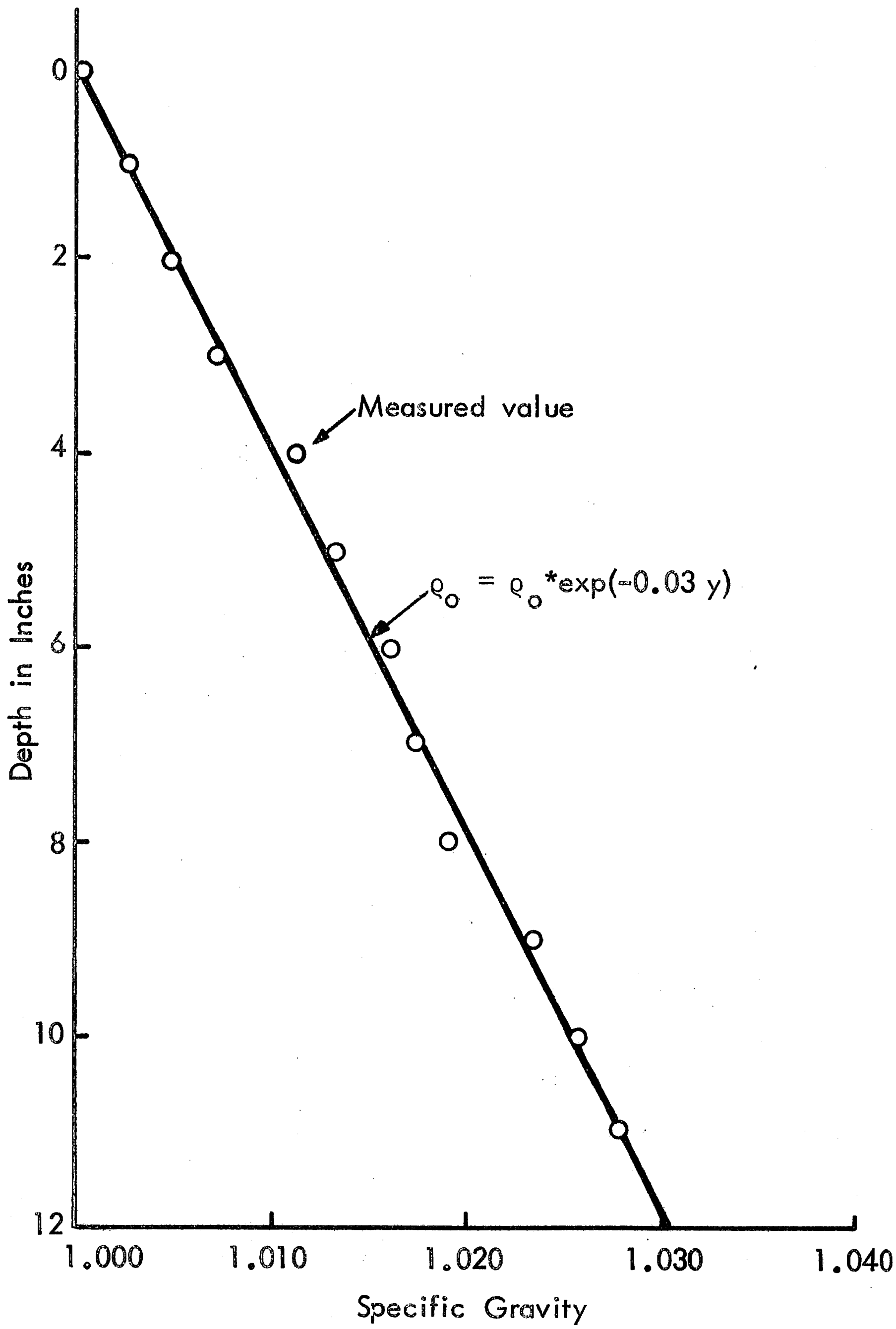

Fig. 10 - A Typical Comparison between the Measured Density Profile and the Ideal Exponential Stratification, $\beta h = 0.015$

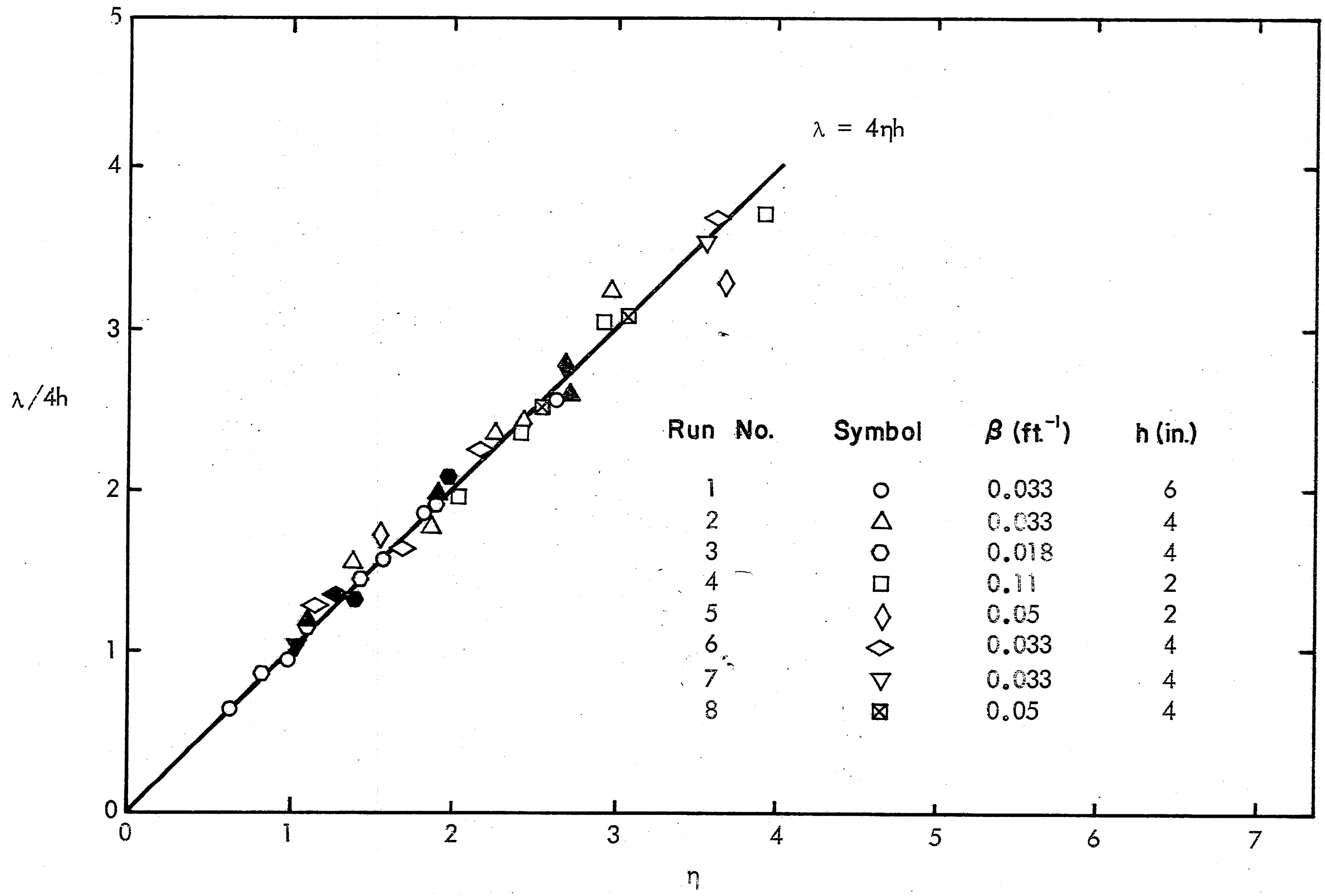

Fig. 11 - Dimensionless Wave Length versus η (filled symbols indicate a free surface and open symbols a solid surface)

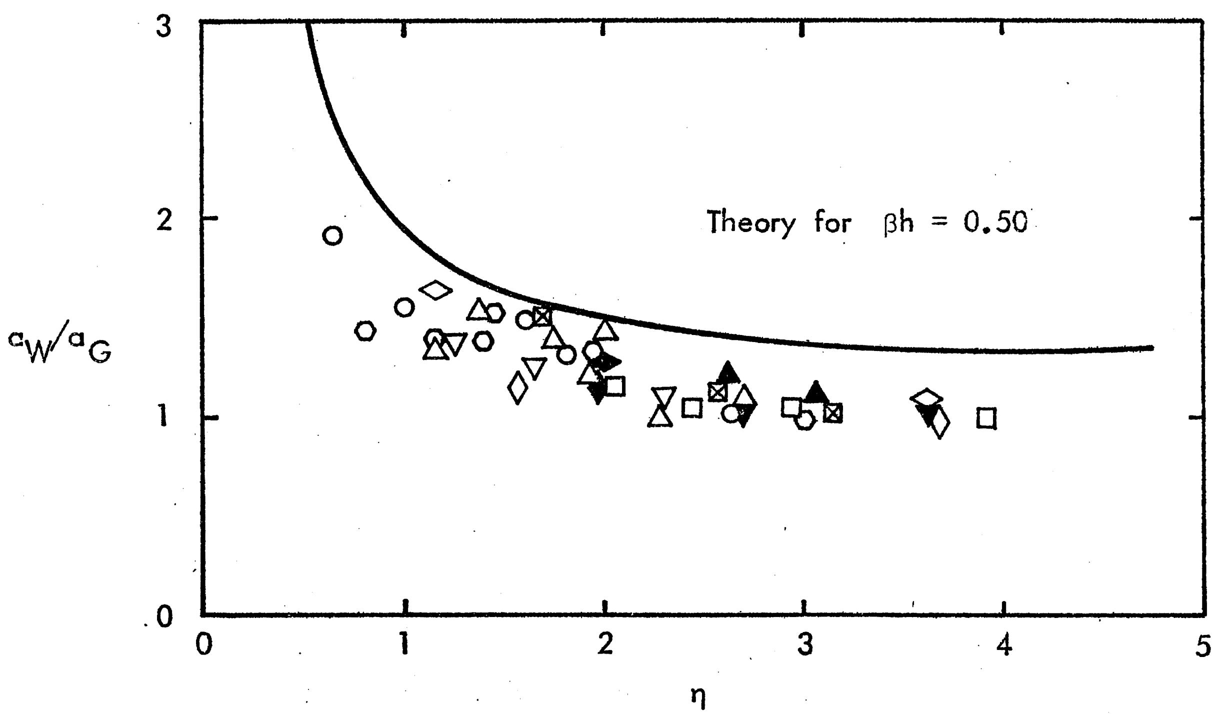

Fig. 12 - Comparison of Computed and Observed Amplitude Ratios (see Fig. 11 for meanings of symbols)

DISTRIBUTION LIST FOR PROJECT REPORT NO. 144
of the St. Anthony Falls Hydraulic Laboratory

Copies	Organization
12	Defense Documentation Center, Cameron Station, Alexandria, Virginia 22314
1	Technical Library, Naval Ship Research and Development Laboratory, Annapolis, Maryland 21402
1	Professor Bruce Johnson, Engineering Department, Naval Academy, Annapolis, Maryland 21402
1	Library, Naval Academy, Annapolis, Maryland 21402
1	Professor W. P. Graebel, Department of Engineering Mechanics, College of Engineering, University of Michigan, Ann Arbor, Michigan 48108
1	Professor T. Francis Ogilvie, Department of Naval Architecture and Marine Engineering, University of Michigan, Ann Arbor, Michigan 48108
1	Professor W. W. Willmarth, Department of Aerospace Engineering, University of Michigan, Ann Arbor, Michigan 48108
1	AFOSR (REM), 1400 Wilson Boulevard, Arlington, Virginia 22204
1	Professor S. Corrsin, Department of Mechanics and Materials Science, The Johns Hopkins University, Baltimore, Maryland 21218
1	Professor R. B. Couch, Department of Naval Architecture and Marine Engineering, The University of Michigan, Ann Arbor, Michigan 48105
1	Professor L. S. G. Kovasznay, Department of Mechanics and Materials Science, The Johns Hopkins University, Baltimore, Maryland 21218
1	Professor O. M. Phillips, Department of Mechanics and Materials Science, The Johns Hopkins University, Baltimore, Maryland 21218
1	Librarian, Department of Naval Architecture, University of California, Berkeley, California 94720
1	Professor P. Lieber, Department of Mechanical Engineering, Institute of Engineering Research, Berkeley, California 94720
1	Professor J. R. Paulling, Institute of Engineering Research, Department of Naval Architecture, University of California, Berkeley, California 94720
1	Professor W. C. Webster, College of Engineering, Department of Naval Architecture, University of California, Berkeley, California 94720
1	Professor J. V. Wehausen, Institute of Engineering Research, Department of Naval Architecture, University of California, Berkeley, California 94720

Copies	Organization
1	Commander, Boston Naval Shipyard, Boston, Massachusetts 02129
1	Director, Office of Naval Research Branch Office, 495 Summer Street, Boston, Massachusetts 02210
1	Commander, Puget Sound Naval Shipyard, Bremerton, Washington 98314
1	Professor G. Birkhoff, Department of Mathematics, Harvard University, Cambridge, Massachusetts 02139
1	Professor G. F. Carrier, Division of Engineering and Applied Physics, Harvard University, Cambridge, Massachusetts 02139
1	Commanding Officer, NROTC Naval Administrative Unit, Massachusetts Institute of Technology, Cambridge, Massachusetts 02139
1	Professor M. A. Abkowitz, Department of Ocean Engineering, Massachusetts Institute of Technology, Cambridge, Massachusetts 02139
1	Professor A. T. Ippen, Department of Civil Engineering, Massachusetts Institute of Technology, Cambridge, Massachusetts 02139
1	Professor Phillip Mandel, Department of Ocean Engineering, Massachusetts Institute of Technology, Cambridge, Massachusetts 02139
1	Professor E. W. Merrill, Department of Chemical Engineering, Massachusetts Institute of Technology, Cambridge, Massachusetts 02139
1	Professor E. Mollo-Christensen, Department of Meteorology, Room 54-1722, Massachusetts Institute of Technology, Cambridge, Massachusetts 02139
1	Professor J. Nicholas Newman, Department of Ocean Engineering, Room 5-324A, Massachusetts Institute of Technology, Cambridge, Massachusetts 02139
1	Commander, Charleston Naval Shipyard, Naval Base, Charleston, South Carolina 29408
1	A. R. Kuhlthau, Director, Research Laboratories for the Engineering Sciences, Thorton Hall, University of Virginia, Charlottesville, Virginia 22903
1	Director, Office of Naval Research Branch Office, 536 South Clark Street, Chicago, Illinois 60605
1	Library, Naval Weapons Center, China Lake, California 93555
1	Professor R. V. Edwards, Division of Chemical Engineering, Case Western Reserve University, Cleveland, Ohio 44106
1	Professor J. M. Burgers, Institute of Fluid Dynamics and Applied Mathematics, University of Maryland, College Park, Maryland 20742

Copies	Organization
1	Professor Pai, Institute for Fluid Dynamics and Applied Mathematics, University of Maryland, College Park, Maryland 20740
1	Acquisition Director, NASA Scientific and Technical Information, P.O. Box 33, College Park, Maryland 20740
1	Technical Library, Naval Weapons Laboratory, Dahlgren, Virginia 22448
1	Dr. C. S. Wells, Jr., Advanced Technology Center, Inc., P.O. Box 6144, Dallas, Texas 75222
1	Dr. R. H. Kraichnan, Dublin, New Hampshire 03444
1	Commanding Officer, Army Research Office, Box CM, Duke Station, Durham, North Carolina 27706
1	Dr. Martin H. Bloom, Polytechnic Institute of Brooklyn, Long Island Graduate Center, Department of Aerospace Engineering and Applied Mechanics, Farmingdale, New York 11735
1	Technical Documents Center, Building 315, U.S. Army Mobility Equipment Research and Development Center, Fort Belvoir, Virginia 22060
1	Technical Library, Webb Institute of Naval Architecture, Glen Cove, Long Island, New York 11542
1	Professor E. V. Lewis, Webb Institute of Naval Architecture, Glen Cove, Long Island, New York 11542
1	Dr. M. Poreh, Technion-Israel Institute of Technology, Department of Civil Engineering, Haifa, Israel
1	Dr. B. N. Pridmore Brown, Northrop Corporation, NORAIR-Division, Hawthorne, California 90250
1	Dr. J. P. Breslin, Davidson Laboratory, Stevens Institute of Technology, Castle Point Station, Hoboken, New Jersey 07030
1	Mr. C. H. Henry, Stevens Institute of Technology, Davidson Laboratory, Castle Point Station, Hoboken, New Jersey 07030
1	Dr. D. Savitsky, Davidson Laboratory, Stevens Institute of Technology, Castle Point Station, Hoboken, New Jersey 07030
1	Dr. A. Strumpf, Davidson Laboratory, Stevens Institute of Technology, Castle Point Station, Hoboken, New Jersey 07030
1	Dr. J. P. Craven, University of Hawaii, 1801 University Avenue, Honolulu, Hawaii 96822
1	Professor J. F. Kennedy, Director, Iowa Institute of Hydraulic Research, State University of Iowa, Iowa City, Iowa 52240

Copies	Organization
1	Professor L. Landweber, Iowa Institute of Hydraulic Research, State University of Iowa, Iowa City, Iowa 52240
1	Professor E. L. Resler, Graduate School of Aeronautical Engineering, Cornell University, Ithaca, New York 14851
1	Dr. Y. H. Pao, Flow Research, Inc., 1819 South Central Avenue, Suite 72, Kent, Washington 98031
1	Dr. D. E. Ordway, Sage Action, Incorporated, P.O. Box 416, Ithaca, New York 14850
1	Professor A. T. Ellis, University of California, San Diego, Department of Aerospace and Mechanical Engineering Science, La Jolla, California 92037
1	Dr. Coda Pan, Mechanical Technology Incorporated, 968 Albany-Shaker Road, Latham, New York 12110
1	Mr. P. Eisenberg, President, Hydronautics, Incorporated, 8210 Pindell School Road, Laurel, Maryland 20810
1	Mr. M. P. Tulin, Hydronautics, Incorporated, 8210 Pindell School Road, Laurel, Maryland 20810
1	Commander, Long Beach Naval Shipyard, Long Beach, California 90802
1	Professor John Laufer, Department of Aerospace Engineering, University Park, Los Angeles, California 90007
1	Professor J. M. Killen, St. Anthony Falls Hydraulic Laboratory, University of Minnesota, Minneapolis, Minnesota 55414
1	Lorenz G. Straub Library, St. Anthony Falls Hydraulic Laboratory, University of Minnesota, Minneapolis, Minnesota 55414
1	Professor J. F. Ripken, St. Anthony Falls Hydraulic Laboratory, University of Minnesota, Minneapolis, Minnesota 55414
1	Professor E. Silberman, Director, St. Anthony Falls Hydraulic Laboratory, University of Minnesota, Minneapolis, Minnesota 55414
1	Superintendent, Naval Postgraduate School, Attn: Library, Monterey, California 93940
1	Professor A. B. Metzner, Department of Chemical Engineering, University of Delaware, Newark, Delaware 19711
1	Technical Library, Naval Underwater Systems Center, Newport, Rhode Island 02840
1	Office of Naval Research, New York Area Office, 207 W. 24th Street, New York, New York 10011

Copies	Organization
1	Professor V. Castelli, Department of Mechanical Engineering, Columbia University, New York, New York 10027
1	Professor H. Elrod, Department of Mechanical Engineering, Columbia University, New York, New York 10027
1	Society of Naval Architects and Marine Engineers, 74 Trinity Place, New York, New York 10006
1	Miss O. M. Leach, Librarian, National Research Council, Aeronautical Library, Montreal Road, Ottawa 7, Canada
1	Technical Library, Naval Coastal System Laboratory, Panama City, Florida 32401
1	Dr. J. W. Hoyt, Naval Undersea R and D Center, Pasadena Laboratory, 3202 E. Foothill Boulevard, Pasadena, California 91107
1	Technical Library, Naval Undersea R and D Center, Pasadena Laboratory, 3203 E. Foothill Boulevard, Pasadena, California 91107
1	Professor A. J. Acosta, Department of Mechanical Engineering, California Institute of Technology, Pasadena, California 91109
1	Professor H. Liepmann, Graduate Aeronautical Laboratory, California Institute of Technology, Pasadena, California 91109
1	Professor M. S. Plesset, Department of Engineering Science, California Institute of Technology, Pasadena, California 91109
1	Professor T. Y. Wu, Department of Engineering Science, California Institute of Technology, Pasadena, California 91109
1	Director, Office of Naval Research Branch Office, 1030 E. Green Street, Pasadena, California 91106
1	Naval Ship Engineering Center, Philadelphia Division, Technical Library, Philadelphia, Pennsylvania 19112
1	Technical Library, Philadelphia Naval Shipyard, Philadelphia, Pennsylvania 19912
1	Professor R. C. MacCamy, Department of Mathematics, Carnegie Institute of Technology, Pittsburgh, Pennsylvania 15213
1	Dr. Paul Kaplan, Oceanics, Inc., Technical Industrial Park, Plainview, New York 11803
1	Technical Library, Naval Missile Center, Point Mugu, California 93441
1	Technical Library, Naval Civil Engineering Laboratory, Port Hueneme, California 93041
1	Commander, Portsmouth Naval Shipyard, Portsmouth, New Hampshire 03801

Copies	Organization
1	Commander, Norfolk Naval Shipyard, Portsmouth, Virginia 23709
1	Dr. H. N. Abramson, Southwest Research Institute, 8500 Culebra Road, San Antonio, Texas 78228
1	Editor, Applied Mechanics Review, Southwest Research Institute, 8500 Culebra Road, San Antonio, Texas 78206
1	Dr. Andrew Fabula, Code 600, Building 106, Naval Undersea R and D Center, San Diego, California 92132
1	Office of Naval Research, San Francisco Area Office, 760 Market Street, Room 447, San Francisco, California 94102
1	Library, Pearl Harbor Naval Shipyard, Box 400, FPO, San Francisco, California 96610
1	Technical Library, Hunters Point Naval Shipyard, San Francisco, California 94135
1	Librarian, Naval Ordnance Laboratory, White Oak, Silver Spring, Maryland 20910
1	Mr. J. Enig, Room 3-252, Naval Ordnance Laboratory, White Oak, Silver Spring, Maryland 20910
1	Fenton Kennedy Document Library, The Johns Hopkins University, Applied Physics Laboratory, 8621 Georgia Avenue, Silver Spring, Maryland 20910
1	Dr. Byrne Perry, Department of Civil Engineering, Stanford University, Stanford, California 94305
1	Professor Milton van Dyke, Department of Aeronautical Engineering, Stanford University, Stanford, California 94305
1	Professor R. C. DiPrima, Department of Mathematics, Rensselaer Polytechnic Institute, Troy, New York 12181
1	Dr. Lee Segel, Department of Mathematics, Rensselaer Polytechnic Institute, Troy, New York 12181
1	Professor J. W. Holl, Ordnance Research Laboratory, Pennsylvania State University, University Park, Pennsylvania 16801
1	Professor J. Lumley, Department of Aerospace Engineering, Pennsylvania State University, University Park, Pennsylvania 16802
1	Dr. J. M. Robertson, Department of Theoretical and Applied Mechanics, University of Illinois, Urbana, Illinois 61803
1	Technical Library, Mare Island Naval Shipyard, Vallejo, California 94592
3	Code 438, Office of Naval Research, Department of the Navy, Arlington, Virginia 22217

Copies	Organization
1	Code 463, Office of Naval Research, Department of the Navy, Arlington, Virginia 22217
1	Code 466, Office of Naval Research, Department of the Navy, Arlington, Virginia 22217
1	Code 468, Office of Naval Research, Department of the Navy, Arlington, Virginia 22217
1	Code 473, Office of Naval Research, Department of the Navy, Arlington, Virginia 22217
1	Code 481, Office of Naval Research, Department of the Navy, Arlington, Virginia 22217
6	Code 2627, Naval Research Laboratory, Washington, D.C. 20390
6	Library, Code 2629 (ONRL), Naval Research Laboratory, Washington, D.C. 20390
1	Code 6170, Naval Research Laboratory, Washington, D.C. 20390
1	Code 4000, Director of Research, Naval Research Laboratory, Washington, D.C. 20390
1	Code 8030 (Maury Center), Naval Research Laboratory, Washington, D.C. 20390
1	Code 8040, Naval Research Laboratory, Washington, D.C. 20390
1	Code 031, Naval Ship Systems Command, Washington, D.C. 20360
1	Code 0341, Naval Ship Systems Command, Washington, D.C. 20360
1	Code 03Z2 (L. Benen), Naval Ship Systems Command, Washington, D.C. 20360
1	Code 03Z1 (J. Schuler), Naval Ship Systems Command, Washington, D.C. 20360
1	Code 2052, Naval Ship Systems Command, Washington, D.C. 20360
1	Code 6034, Naval Ship Engineering Center, Center Building, Prince George's Center, Hyattsville, Maryland 20782
1	Code 6101E, Naval Ship Engineering Center, Center Building, Prince George's Center, Hyattsville, Maryland 20782
1	Code 6110, Naval Ship Engineering Center, Center Building, Prince George's Center, Hyattsville, Maryland 20782
1	Code 6114, Naval Ship Engineering Center, Center Building, Prince George's Center, Hyattsville, Maryland 20782

Copies	Organization
1	Code 6120E, Naval Ship Engineering Center, Center Building, Prince George's Center, Hyattsville, Maryland 20782
1	Code 6136, Naval Ship Engineering Center, Center Building, Prince George's Center, Hyattsville, Maryland 20782
1	Dr. A. Powell (Code 01), Naval Ship Research and Development Center, Bethesda, Maryland 20034
1	Mr. W. M. Ellsworth (Code 11), Naval Ship Research and Development Center, Bethesda, Maryland 20034
1	Dr. W. E. Cummins (Code 15), Naval Ship Research and Development Center, Bethesda, Maryland 20034
1	Dr. H. R. Chaplin (Code 16), Naval Ship Research and Development Center, Bethesda, Maryland 20034
1	Mr. G. H. Gleissner (Code 18), Naval Ship Research and Development Center, Bethesda, Maryland 20034
1	Mr. R. Wermter (Code 152), Naval Ship Research and Development Center, Bethesda, Maryland 20034
1	Dr. W. B. Morgan (Code 154), Naval Ship Research and Development Center, Bethesda, Maryland 20034
1	Mr. J. B. Hadler (Code 156), Naval Ship Research and Development Center, Bethesda, Maryland 20034
1	Library (Code 5641), Naval Ship Research and Development Center, Bethesda, Maryland 20034
1	Mr. S. F. Crump (Code 1505), Naval Ship Research and Development Center, Bethesda, Maryland 20034
1	Dr. P. Pien (Code 1521), Naval Ship Research and Development Center, Bethesda, Maryland 20034
1	Mr. Paul Granville (Code 1541), Naval Ship Research and Development Center, Bethesda, Maryland 20034
1	Mr. J. McCarthy (Code 1552), Naval Ship Research and Development Center, Bethesda, Maryland 20034
1	Dr. Nils Salvesen (Code 1552), Naval Ship Research and Development Center, Bethesda, Maryland 20034
1	Dr. M. Strasberg (Code 1901), Naval Ship Research and Development Center, Bethesda, Maryland 20034
1	Code 03, Naval Air Systems Command, Department of the Navy, Washington, D.C. 20360

Copies	Organization
1	AIR 5301, Naval Air Systems Command, Department of the Navy, Washington, D.C. 20360
1	AIR 604, Naval Air Systems Command, Department of the Navy, Washington, D.C. 20360
1	Code ORD 03, Naval Ordnance Systems Command, Department of the Navy, Washington, D.C. 20360
1	Code ORD 035, Naval Ordnance Systems Command, Department of the Navy, Washington, D.C. 20360
1	Code ORD 05413, Naval Ordnance Systems Command, Department of the Navy, Washington, D.C. 20360
1	Code ORD 9132, Naval Ordnance Systems Command, Department of the Navy, Washington, D.C. 20360
1	CNM PM-1, Strategic Systems Project Office, Department of the Navy, Washington, D.C. 20360
1	Technical Division (CNM PM 11-20), Deep Submergence Systems Project Office, Department of the Navy, Washington, D.C. 20360
1	Oceanographer of the Navy, Washington, D.C. 20390
1	Commander, Naval Oceanographic Office, Washington, D.C. 20390
1	Dr. A. L. Slafkosky, Scientific Adviser, Commandant of the Marine Corps (CODE AX), Washington, D.C. 20380
1	Librarian Station 5-2, Coast Guard Headquarters, NASSIF Building, 400 - 7th Street, S.W., Washington, D.C. 20591
1	Office of Research and Development, Maritime Administration, 441 G Street, N.W., Washington, D.C. 20235
1	Division of Ship Design, Maritime Administration, 441 G Street, N.W., Washington, D.C. 20235
1	National Science Foundation, Engineering Division, 1800 G Street, N.W., Washington, D.C. 20550
1	Dr. G. Kulin, National Bureau of Standards, Washington, D.C. 20234
1	Science and Technology Division, Library of Congress, Washington, D.C. 20234
1	Chief of Research and Development, Office of Chief of Staff, Department of the Army, Washington, D.C. 20310
1	Professor A. Thiruvengadam, Department of Mechanical Engineering, The Catholic University of America, Washington, D.C. 20017

Unclassified
Security Classification

14 KEY WORDS	LINK A		LINK B		LINK C	
	ROLE	WT	ROLE	WT	ROLE	WT
Internal waves						
Wave generator						
Image method						
Wavemaking singularities						

DD FORM 1 NOV 65 1473 (BACK)
S/N 0101-807-6821

Unclassified
Security Classification

A-31409